Systematic evaluation of additive loading effects on burn rate, density, and mass flow in PVC/AP composite solid propellants

Bansal, Lakshay; Jindal, Prakhar

DOI
10.1016/j.ast.2025.110452

Publication date
2025

Document Version
Final published version

Published in
Aerospace Science and Technology

Citation (APA)
Bansal, L., & Jindal, P. (2025). Systematic evaluation of additive loading effects on burn rate, density, and mass flow in PVC/AP composite solid propellants. *Aerospace Science and Technology*, *164*, Article 110452. https://doi.org/10.1016/j.ast.2025.110452

Aerospace Science and Technology 164 (2025) 110452

Contents lists available at ScienceDirect

Aerospace Science and Technology

journal homepage: www.elsevier.com/locate/aescte

Systematic evaluation of additive loading effects on burn rate, density, and mass flow in PVC/AP composite solid propellants

Lakshay Bansal [a], Prakhar Jindal [b,*]

[a] School of Chemical Sciences, University of Illinois, Urbana-Champaign, USA
[b] Space System Engineering, TU Delft, The Netherlands

ARTICLE INFO

Communicated by Suresh Menon

Keywords:
Composite solid propellant
Ammonium perchlorate
Polyvinyl chloride
Di-butyl phthalate
Burn rate

ABSTRACT

Solid composite propellants continue to play a key role in space and defense propulsion due to their high energy density, ease of handling, and manufacturing scalability. While several studies have investigated the effect of individual additives on propellant performance, most are limited to a fixed weight percentage or particle size, making it difficult to derive comprehensive design guidelines. This study presents a systematic comparative investigation into the influence of various additives (Al, Fe_2O_3, $CuCr_2O_4$, and thermite combinations) and their particle sizes/loadings on the performance of polyvinyl chloride (PVC)/ammonium perchlorate (AP)-based composite propellants. Over 30 distinct formulations were experimentally characterized for burn rate, density, adiabatic flame temperature (AFT), and mass flow rate to establish comprehensive performance trends and trade-offs. The results demonstrate that smaller metal particle sizes and higher additive loadings generally enhance burn rate and mass flow, indicative of catalytic effects. Thermochemical analysis supports the significant exothermic contribution of the Al–Fe_2O_3 thermite reaction (–851.5 kJ/mol) to increased combustion energy. Furthermore, calculated oxidizer-balance percentages correlate with AFT and burn rate, with near-stoichiometric formulations exhibiting peak performance. The highest theoretical thrust (~73 N) was predicted for a Fe_2O_3-rich formulation aligning with high energy and burn rate. While the catalytic mechanisms of these additives are known, the key contribution of this work lies in the extensive, comparative dataset across a wide range of propellant compositions. This broad dataset serves as a valuable resource for optimizing propellant formulations, validating combustion models, and guiding future propellant design.

1. Introduction

Solid propellants for decades have been the driving force for most space launch vehicles and ballistic missiles due to their high thrust-to-weight ratio compared to other rocket propulsion systems [1]. Composite solid propellants (CSP) have long served as the primary energetic material for heavy-duty solid rocket motor (SRM), consisting of a crystalline oxidizer and high-energy fuel, along with various other elements like burn rate catalyst, cross-linking and curing agent. The formulations of these solid propellants can be as simple as an oxidizer-fuel system where the binder also acts as the fuel. It can be a complex, multi-component formulation incorporating energetic additives to tailor specific performance characteristics [2–5]. Different formulations with various ingredients have been tested and proven, but ammonium perchlorate (AP) based compositions have always topped the list. Due to the high oxygen content, thermal stability, and the capability of producing very high specific impulse at low decomposition temperature, AP has superior ballistics, a highly energetic nature, and better combustion characteristics in comparison to its competitors, like ammonium nitrate, ammonium dinitramide, etc. [6–10]. Ammonium perchlorate is compatible with different fuels and binders, and thus can be used without concern about stability issues caused by molecular interaction between the various ingredients of the composition. For example, hydroxy-terminated polybutadiene (HTPB), which is a polymeric fuel/binder compound, and polyvinyl chloride (PVC), a well-known plastic binder and energetic fuel, are the most used fuel/binder compounds, along with many others, depending on the mission objective [3,11,12]. Polyvinyl chloride is an excellent combination of fuel-binder, as it requires no special storage conditions, plus its low cost and easy availability make it an excellent choice for solid as well as hybrid rocket systems [13].

The new market for solid rocket propellants (SRP) is not just limited

* Corresponding author.
E-mail address: p.jindal@tudelft.nl (P. Jindal).

https://doi.org/10.1016/j.ast.2025.110452
Received 19 May 2025; Accepted 6 June 2025
Available online 6 June 2025

to conventional space research applications, but with the increasing interest in space tourism, finding economic, reliable, and safe propellant compositions is becoming an attractive sector of research in rocketry and propulsion. The increased demand for enhancing the performance characteristics, such as burn rate (r_b) of the conventional composition by extracting higher energy output, has become a major research challenge. This can be done in various ways, such as changing the internal geometry of the solid rocket motor, altering the particle size of the ingredients, and using enhanced ingredients (surface-treated fuel and oxidizer particles) [14]. Eq. (1) is a well-known relation that represents the empirical Vieille's law where burn rate (r_b) is a function of chamber pressure (P) to the power pressure index (n) and temperature coefficient (a) [1].

$$r_b = a.P^n \tag{1}$$

But the easiest way is to add energy-dense additives, such as metals, metalloids, transition metal oxides, along with metal/metal-oxide thermite combinations [15–19]. Manash et al. conducted a comparative study between HTPB and PVC as fuels, and it was observed that adding 3 % of ferric oxide as a catalyst significantly increased the burn rate for AP-based compositions [16]. Another study conducted by Gou et al. showed that adding copper chromite can increase the density as well as positively enhance the thermal characteristics of AP-based solid propellant compositions, subsequently resulting in higher energy release. An approximate 28 % increase in burn rate was seen when $CuCr_2O_4$ was incorporated [20]. Researchers have tested various thermite combinations, such as Ni/Al/Fe_2O_3 [21] and Al/CuO [22] to investigate their influence on the performance of solid propellants. It was found that the addition of thermites can effectively enhance the ignition as well as the burning characteristics. Also, changing the ambient conditions, such as ambient temperature, can affect the mechanical as well as combustion characteristics of the solid propellant [23,24]. Another study conducted on the effects of additives on the burn rate of amateur propellant compositions such as sucrose and KNO_3 showed that additions of metallic and inorganic catalyst can alter the burn rate even when incorporated at a reduced oxidizer loading [25].

Although the catalytic mechanisms of additives such as ferric oxide, aluminum, and copper chromite in AP-based propellants are well documented, most existing studies focus on individual additives or fixed weight percentages, typically limited to 1 % or 2.5 % by weight, which restricts the ability to identify broader trends or optimize formulations. This study addresses that gap by systematically evaluating a wide range of additive types, loadings, and particle sizes, generating a comprehensive dataset that correlates burn rate, density, and mass flow rate across diverse propellant compositions. To the best of the authors' knowledge, this is the first work to comprehensively link how variations in additive type, concentration, and particle size collectively influence burn rate and density and how these changes affect mass flow rate. Understanding these combined effects, including specific investigations into particle size in ammonium perchlorate and PVC-based formulations, provides crucial insights into how low density coupled with high burn rate (and vice versa) impacts mass flow, a significant factor in propellant performance and efficiency. These findings offer valuable guidance for optimizing additive loadings and selecting the most effective catalytic additives, ultimately advancing the design and combustion characteristics of AP-based composite solid propellants.

2. Materials and methods

2.1. Material

Polyvinyl chloride (CDH fine chemical) ammonium perchlorate (CDH fine chemical and array >99.8 %), dibutyl phthalate (Sigma Aldrich and array >99 %), aluminum powder (make- Qualikems, purity >99.97 %), red iron oxide (make- Qualikems, purity >98.5 %), copper chromite (Sigma Aldrich and 70 %< array >90 %). All these ingredients were commercially purchased and used without any further processing. The ingredients used to prepare the composite propellant strands, along with their properties, are mentioned in Table 1. Polyvinyl chloride melts and hardens quickly when heated above 100 °C. Thus, Di-butyl Phthalate is used as the plasticizer with PVC to soften the composition and provide the required elasticity to mold, cast, and cut into the strand form with the required dimensions. This also provides mechanical strength after the strands cure and helps with binding other constituents of the composition.

2.2. Compositions and preparation

All the tested compositions are mentioned in the following tables. Table 2 represents the compositions with different weight percent (wt. %) and particle size of AP (as oxidizer). Table 3 represents compositions with different ambient temperature testing scenarios. Table 4 represents the compositions with different additives, along with their wt. % in the compositions. Table 5 represents the compositions with copper chromite as an additive of varying particle sizes. Although preliminary screening indicated that a 75 % oxidizer content resulted in the highest burn rate among the tested oxidizer-to-fuel ratios, 70 % AP and 30 % PVC-DBP were selected as the base composition (C1) for further additive-based studies. This decision was based on ensuring consistent strand integrity, manageable burn rate, and processability across a large number of formulations. Higher oxidizer loading led to weaker mechanical strength in the strands, complicating handling and testing. Therefore, 70 % oxidizer was adopted as a balanced and reliable baseline.

For aluminum additive compositions, loading values of 2.5 %, 5 %, 7.5 %, and 10 % by weight were selected. These increments were chosen to reflect a meaningful range that balances literature benchmarks with practical processing constraints. Values above 10 % tend to destabilize the slurry and reduce strand cohesion, while values below 2.5 % show minimal combustion enhancement. The chosen increments also allow evaluation of non-linear trends in performance metrics. The variables inherent to the propellant strand formulation process, such as mixing time and temperature, sequence in which the ingredients were added, curing duration and temperature, were maintained consistently for all compositions.

The required amount of ammonium perchlorate, PVC, and de-moisturized DBP was measured using a weighing balance and mixed in a 100 ml glass beaker. This mixture and the additives were thoroughly stirred for 3 - 4 h using a magnetic stirrer plate and a stirring bar. The ratio of PVC and de-moisturized DBP was kept at 1:1 [16]. Due to the volatile nature of DBP, a higher wt. % of de-moisturized DBP was used, as only 8–10 % would remain after the mixing process, and it will act as a process control agent during the stirring process. Ammonium perchlorate of particle size under 50 μm (fine AP) and particle size above 250 μm (coarse AP) were used to get a higher solid loading, faster ignition, and stable burning of the propellant strand [26]. The ratio between the coarse and fine AP was 1:3 to constitute for oxidizer loading. The particle size of 30 μm - 45 μm was chosen for PVC. PVC melts at 100 °C, that is, during the curing process (discussed later), thus its particle size is not of much significance. For aluminum powder, particles under 45 μm were used for the current study. Comparable particle size of 40 μm – 70 μm for both the ceramic oxidizers was used to establish a comparative trend in the burn rate of the tested compositions.

After the mixing and stirring process, the propellant slurry was poured into a greased 50 mm × 50 mm × 10 mm metallic tray, which was greased using Metroark grease to avoid the slurry from sticking to the tray. The mixture was then kept for the curing process at 100 $^{\circ}C \pm 1$ °C in the oven for 20 h, after which the curing tray was removed from the oven and the propellant slurry was allowed to cool at room temperature for 24 h. This also allowed the cured propellant strands to attain appropriate mechanical strength [16]. Fig. 1 illustrates some of the compositions for solid propellants that were investigated in the present study. After the propellant slurry had cooled down to room temperature

Table 1
Constituents of the compositions with their physical and chemical properties.

Constituents	Phase at NTP	Chemical Formula	Molar Mass (g/mol)	Density (g/cm^3)	Boiling point (°C)	Melting Point (°C)
Polyvinyl chloride	Solid	$(C_2H_3Cl)_n$	62.496n	1.4	—	100 - 270
Di-butyl phthalate	Liquid	$C_{16}H_{22}O_4$	278.34	1.05	340–35	—
Ammonium perchlorate	Solid	NH_3ClO_4	117.49	1.95	—	~200
Aluminum	Solid	Al	26.98	2.70	2470	660.3
Ferric Oxide	Solid	Fe_2O_3	159.69	5.24	—	—
Carbon	Solid	C	12.011	0.65	—	—
Copper chromite	Solid	$CuCr_2O_4$	231.538	5.22	—	—

Table 2
Wt. % of different ingredients with variable conditions.

Composition ID	Oxidizer	Fuel	Variation	
C 1	70.0	30.0		
C 2	72.5	27.5		
C 3	75.0	25.0	NA	Varying the oxidizer fuel ratio
C 4	77.5	22.5		
C 5	80.0	20.0		
C 6	70.0	30.0	<50	Different oxidizer particle sizes (μm)
C 7			50–150	
C 8			150–250	
C 9			>250	

Table 3
Various ambient temperatures.

Composition	Oxidizer	Fuel	Different atmospheric temperatures (°C)
C 10	70.0	30.0	30 (303.15 K)
C 11			40 (313.15 K)
C 12			50 (323.15 K)
C 13			60 (333.15 K)
C 14			70 (343.15 K)

Table 4
Composition with different additives with various wt. %.

Composition	Oxidizer	Fuel	Additive		
			Al	Fe_2O_3	$CuCr_2O_4$
C 15	70	27.5	2.5	0	
C 16		25	5		
C 17		22.5	7.5		
C 18		20	10		
C 19		23	6	2	
C 20		18	10	2	0
C 21		29	0	1	
C 22		28		2	
C 23		27		3	
C 24		26		4	
C 25		25		5	
C 26		29			1
C 27		28			2
C 28		27		0	3
C 29		26			4
C 30		25			5

Table 5
Composition with Copper Chromite as additives with varying particle size.

Composition	Oxidizer	Fuel	Particle size (μm)
C 31	70	25	<40
C 32			40–70
C 33			70–100
C 34			100–130

and had hardened, the propellant was then removed from the tray and carefully cut using a Surgical #10 disposable blade scalpel to obtain propellant strands with a dimension of 60 mm × 10 mm × 10 mm. A syringe needle was used to make holes at the required locations (A1 and A2) in the strand, and the nichrome wire was then pierced through these holes. A detailed description of the nichrome wire-based initiator setup and testing setup is given in Sections 2.3 and 2.4.

A $CaCO_3$-based desiccator was used to store the prepared propellant strands to prevent the strands from absorbing any moisture and to remove any moisture that might have been absorbed during the preparation process. To ensure dimensional uniformity, each propellant strand was carefully measured and sanded down (if needed) to the dimensions of our interest. Four strands from each composition were selected for linear burn rate testing. All experimental procedures were conducted under ambient laboratory conditions (temperature 25 ± 2 °C, relative humidity ~40–50 %).

2.3. Initiator setup

An electrical pyrotechnic initiator system, based on the bridge wire concept (as depicted in Fig. 2) that was developed for previous experiments was used to provide the initial thermal energy to ignite the propellant strand [25]. The initiator system utilized a nichrome wire, measuring 70 mm in length and 0.6 mm in diameter, as the bridge wire, which was pierced into the strand at one end. An on-off bell switch was incorporated into the system to control the onset and stop of the electrical power. The two ends of the nichrome wire were connected to the terminals of a 12 V, 7.5 Ah battery to provide this power, using a 2 mm copper wire. To facilitate safe operation, a distance of 10 m from the firing setup was maintained.

2.4. Burn rate testing

The nichrome wires at point A1 and A2 were connected to an electrical circuit that included two LED bulbs (B1 and B2), powered by two 1.5 V AAA batteries connected in series, as seen in Fig. 2. The distance between A1 and A2 was fixed at 60 mm for all the compositions, and the time taken for this 60 mm length of strand to burn was taken as the burn time.

The linear burn rates of all the compositions were measured under standard pressure and temperature conditions. To ensure linear burning and prevent side ignition, the side surfaces of the propellant strands were coated with polyethylene enamel, acting as an inhibitor. The burning surface of a solid propellant typically regresses in a direction perpendicular to the surface [1]. The burn rate tests were conducted in a fume hood to provide a controlled environment and proper ventilation, minimizing the risk of inhaling any gases produced during combustion. To replicate the initial condition and stimulate the launch sequence of rocket, where the combusting gases pressurize the combustion chamber of motor, the tests were performed under open atmospheric conditions.

Each propellant strand was positioned vertically in the fume hood and ignited using an electrical pyrotechnic initiator system. Before initiating ignition, the secondary circuit with two indicator bulbs was activated. When the nichrome wire at location A1 melted due to the

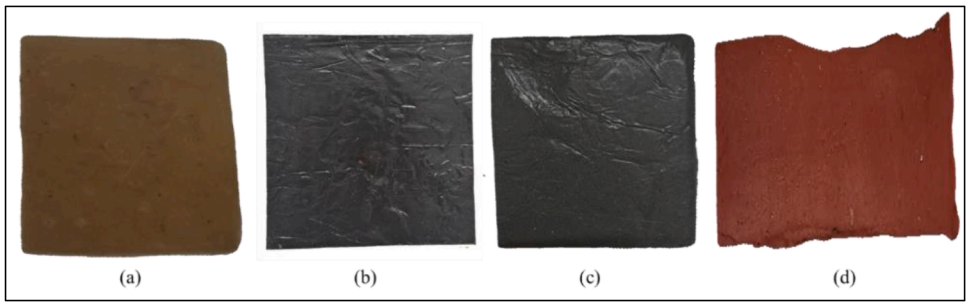

Fig. 1. Example images of cured AP/PVC propellant samples with (a) Base sample with no additives (b) $CuCr_2O_4$ (c) Aluminum (d) Red Iron oxide.

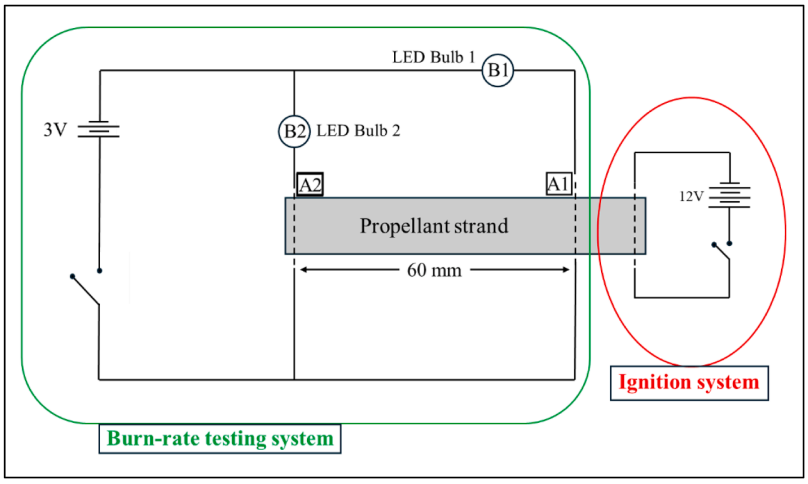

Fig. 2. Line diagram for burn rate testing and ignition system.

propellant charge burning around it, the connected LED bulb (B1) turned off, marking the beginning of combustion at A1. Similarly, the second LED bulb (B2) switched off once the nichrome wire at A2 melted. The entire combustion process was recorded on video, and the elapsed time between the two LED bulbs turning off was determined by reviewing the footage at 0.5x speed. This duration was used as the burn time for the 60 mm length of the propellant strand. All four strands from each composition were tested in this manner to calculate an average linear burn rate.

3. Experimental results and discussions

Various compositions were tested to investigate the effects of incorporating different weight percentages and particle sizes of metallic and metal oxide additives on the burn rate, density, and theoretical adiabatic flame temperature (AFT) of AP/PVC-based composite solid propellant strands. The results revealed that both the burn rate and density generally increased with the addition of these additives. However, the AFT exhibited mixed trends, depending on the specific additive and its loading in the compositions. Table 6 represents the numeric values for burn time, burn rate, along with the standard deviation (Stand. Dev.) (rounded off to the nearest 10×10^3). The standard deviation for all the propellant compositions was found to be within acceptable limits. The maximum and the minimum standard deviation for the propellant were found to be 0.0274 and 0.0082, respectively. Table 6 also includes the percentage change in the burn rate and adiabatic flame temperatures of different compositions with various additives. The mass flow rate for the tested composition was also calculated and discussed in Section 3.1, along with the equations that were used for the calculation.

3.1. Burn rate

Fig. 3 presents the burn rate and burn time trends for various AP and PVC-based solid propellant compositions, while Fig. 4 illustrates the percentage change in burn rate through bar graphs with numeric labels for clarity. The baseline composition (Composition 1), formulated with a standard oxidizer-to-fuel ratio of 70:30, exhibited a burn rate of 1.32 mm/s. Composition 25 recorded the highest burn rate of 6.27 mm/s, marking a significant 375 % improvement over the baseline. In contrast, the lowest improvement was observed in the composition having 85 % oxidizer loading, which showed a burn rate of 1.37 mm/s with only a 3.79 % increase in the burn rate.

For compositions with increasing oxidizer content, Fig. 3(a) shows that the burn rate initially increased as the oxidizer weight percentage was increased, reaching a peak at 75 % with a burn rate of 1.64 mm/s. Beyond this loading, a decline in burn rate was observed. This can be attributed to the fact that optimal thermal output occurs near the stoichiometric ratio, which in our compositions is slightly deviated due to the presence of plasticizer [27]. Increasing the oxidizer wt. % beyond 75 % led to a reduction in burn rate, with values of 1.37 mm/s for the composition with 80 % oxidizer loading. This is likely due to the extra oxidizer absorbing additional heat to decompose and produce free available oxygen. Also, the reduced amount of PVC led to comparatively low heat energy production, which decelerated the decomposition mechanism of the AP, resulting in higher burn times and reduced burn rates. The effect of ambient temperature on burn rate is illustrated in Fig. 3(b). For example, Composition 10 tested at 30 °C recorded a burn rate of 1.43 mm/s, whereas Composition 14 tested at 70 °C demonstrated a burn rate of 2.02 mm/s, representing a 53.03 % increase over the baseline. This phenomenon can be explained through the Arrhenius relation presented below as Eq. (2). Here, k represents the rate constant

Table 6
Burn rate and burn time for all the tested compositions with their standard deviations.

Composition ID	Burn time (s)	Stand. Dev.	Burn rate (mm/s)	Percentage change (%)	Adiabatic Flame Temp. (K)
C 1	***45.45***	***0.0124***	***1.32***	***BASE***	2652.31
C 2	39.01	0.0098	1.55	17.42	2689.19
C 3	36.59	0.0233	1.64	24.24	2704.37
C 4	38.18	0.0217	1.58	19.70	2698.04
C 5	43.80	0.0167	1.37	3.79	2670.55
C 6	29.13	0.0143	2.06	56.06	
C 7	34.48	0.0079	1.74	31.82	2652.31*
C 8	38.71	0.0198	1.55	17.42	
C 9	43.80	0.0237	1.37	3.79	
C 10	41.93	0.0221	1.43	8.33	2653.25
C 11	38.61	0.0212	1.55	17.42	2656.13
C 12	36.76	0.0094	1.63	23.48	2658.71
C 13	34.97	0.0233	1.71	29.55	2661.33
C 14	29.58	0.0156	2.02	53.03	2663.97
C 15	40.54	0.0172	1.48	12.12	2812.77
C 16	39.47	0.0271	1.52	15.15	2939.16
C 17	34.68	0.0162	1.73	31.06	3045.69
C 18	28.71	0.0134	2.09	58.33	3139.16
C 19	27.40	0.0133	2.19	65.91	1979.45
C 20	21.58	0.0156	2.78	110.61	2063.14
C 21	35.93	0.0172	1.67	26.52	1810.15
C 22	28.99	0.0178	2.07	56.82	1891.68
C 23	20.07	0.0211	2.99	126.52	1970.54
C 24	13.67	0.0145	4.39	232.58	2046.59
C 25	9.57	0.0153	6.27	375.00	2119.67
C 26	23.35	0.0274	2.57	94.70	
C 27	20.96	0.0231	2.86	116.97	
C 28	18.81	0.0112	3.19	141.67	
C 29	16.90	0.0142	3.55	168.91	
C 30	15.23	0.0099	3.94	198.48	#
C 31	11.86	0.0219	5.06	283.34	
C 32	15.23	0.0082	3.94	198.48	
C 33	20.91	0.0165	2.87	117.42	
C 34	30.61	0.0223	1.96	48.48	

* The AFT for these compositions is the same as that for C1, as there was a change in the particle size with no change in wt. % of ingredients. # The data for $CuCr_2O_4$ is not available in the NASA CEA program.

of the reaction, A is the pre-exponential factor, E_a is the activation energy, R is the universal gas constant, and T is the temperature in Kelvin.

$$k = A.e^{\frac{-E_a}{RT}} \tag{2}$$

As the temperature increases, which in our case is the initial ambient temperature. The exponent term is smaller and hence less negative. This in turn increases the overcome the activation energy barrier faster, hence leading to faster reaction and enhanced burn rate.

The influence of oxidizer particle size is highlighted in Fig. 3(c). A clear inverse relationship between particle size and burn rate was observed, with compositions utilizing AP particles under 50 μm achieving the highest burn rate for particle size scenarios. The percentage improvement in burn rate decreased from 56.06 % to just 3.79 % as particle size increased. As the particle size decreases, the surface area to volume ratio of the particle increases, and increased surface area is directly proportional to increased reactive surface and thus improved reactive interface. This means that, at the particle level, the flame can propagate more rapidly over a larger area. As a result, the combustion reaction accelerates locally, leading to an increase in the burn rate with a decrease in ingredient particle size [28]. Similar action can be observed when $CuCr_2O_4$ of different particle sizes was included in the compositions. The burn rate went from 5.06 mm/s (283.34 % improvement from the base composition) for the composition with $CuCr_2O_4$ of particle size under 40 μm to 1.96 mm/s when the particle size was between 100–130 μm, as seen in Fig. 3(e). Although the specific surface area of the $CuCr_2O_4$ used in this study was not experimentally measured, prior literature indicates that nano-sized $CuCr_2O_4$ particles synthesized through wet chemical methods typically exhibit surface areas in the range of 30–60 m^2/g [20,29,30]. This high surface area promotes adsorption of decomposition intermediates and enhances catalytic reactivity by increasing the number of active sites for redox reactions. The observed performance enhancement in our formulations containing fine $CuCr_2O_4$ particles aligns with this expected behavior, further validating its catalytic effectiveness.

Metal oxides are well-established catalysts, known for their ability to accelerate the decomposition of various oxidizers, including ammonium perchlorate, by acting as oxygen carriers. Owing to their multiple oxidation states, these oxides offer a high density of active sites where redox reactions can readily occur. Additionally, their substantial heat capacity allows them to act as thermal reservoirs or hot spots that absorb heat during the combustion of the preceding charge and subsequently transfer it to unreacted regions. This heat transfer facilitates faster ignition of the successive propellant layers even before the convective heat from the preceding layer arrives, effectively enhancing the overall reaction rate. It can be seen from Fig. 3(d) and (f) that the compositions containing metal oxide additives showed the most substantial enhancements in burn rate. Compositions 21 to 25, which included Fe_2O_3 as an additive, demonstrated a burn rate improvement from 26.56 % at 1 % additive loading to 375 % at 5 %, reaching a maximum burn rate of 6.27 mm/s. During the redox cycling of the Fe_2O_3, it gets reduced to Fe_3O_4 by losing an electron. This reduction process is an exothermic phenomenon that contributes additional energy to the overall heat release of the propellant combustion. On reduction, the iron oxide molecule releases nascent oxygen available for the fuel to start its combustion, even before the primary oxidizer decomposes. Combining all these kinetic mechanisms thereby accelerates the oxidiser's decomposition and enhances the burn rate [31,32]. Similar catalytic behavior was observed in compositions 26 to 34 containing $CuCr_2O_4$, showing a maximum improvement of 283.34 % with a burn rate of 5.06 mm/s. $CuCr_2O_4$ possesses a high surface area, which facilitates the adsorption of intermediate products from the decomposing oxidizer. This surface interaction helps stabilize the transition states associated with the reduction of Cu^{2+} and Cr^{6+} ions. The exothermic nature of these redox reactions contributes additional heat to the system, thereby lowering the energy barrier required to break chemical bonds in the oxidizer. Together, these effects enhance the decomposition rate of the oxidizer and contribute to a higher overall burn rate [20,29,30].

Compositions incorporating aluminum as an additive exhibited relatively modest enhancements in burn rate compared to those with metal oxides or thermite. The composition containing 2.5 % aluminum showed only a 12.12 % increase over the baseline, with a burn rate of 1.48 mm/s. whereas, when 10 % aluminum was added, the burn rate increased to 2.08 mm/s, marking 58.33 % improvement. In case of aluminum combustion, significant thermal energy is produced due to its high energy density, with a heat of combustion of approximately 31 MJ/kg [33]. Also, the ceramic oxidizer produced as a result of aluminum combustion can transfer the heat to the adjacent unreacted charge, acting as a thermal hotspot. Aluminum is known to produce high flame temperatures, which in turn accelerate the decomposition of the oxidizer. The combined effect of the hot reaction product and high temperature flames together accounts for the increase in burn rate [34,35].

Significant improvements in burn rate were observed in compositions incorporating thermite additives, particularly those based on Al–Fe_2O_3. The thermite reaction between aluminum and iron oxide is highly exothermic, releasing approximately −851.5 kJ/mol of energy according to standard enthalpies of formation. This intense heat output not only sustains combustion but also preheats adjacent unreacted material, accelerating ignition propagation at the particle level. In Composition 19, which used Al–Fe_2O_3 at the stoichiometric ratio ($\Phi = 1$), a 65.91 % increase in burn rate was recorded. The exothermic redox reaction produces molten iron and aluminum oxide, and the presence of

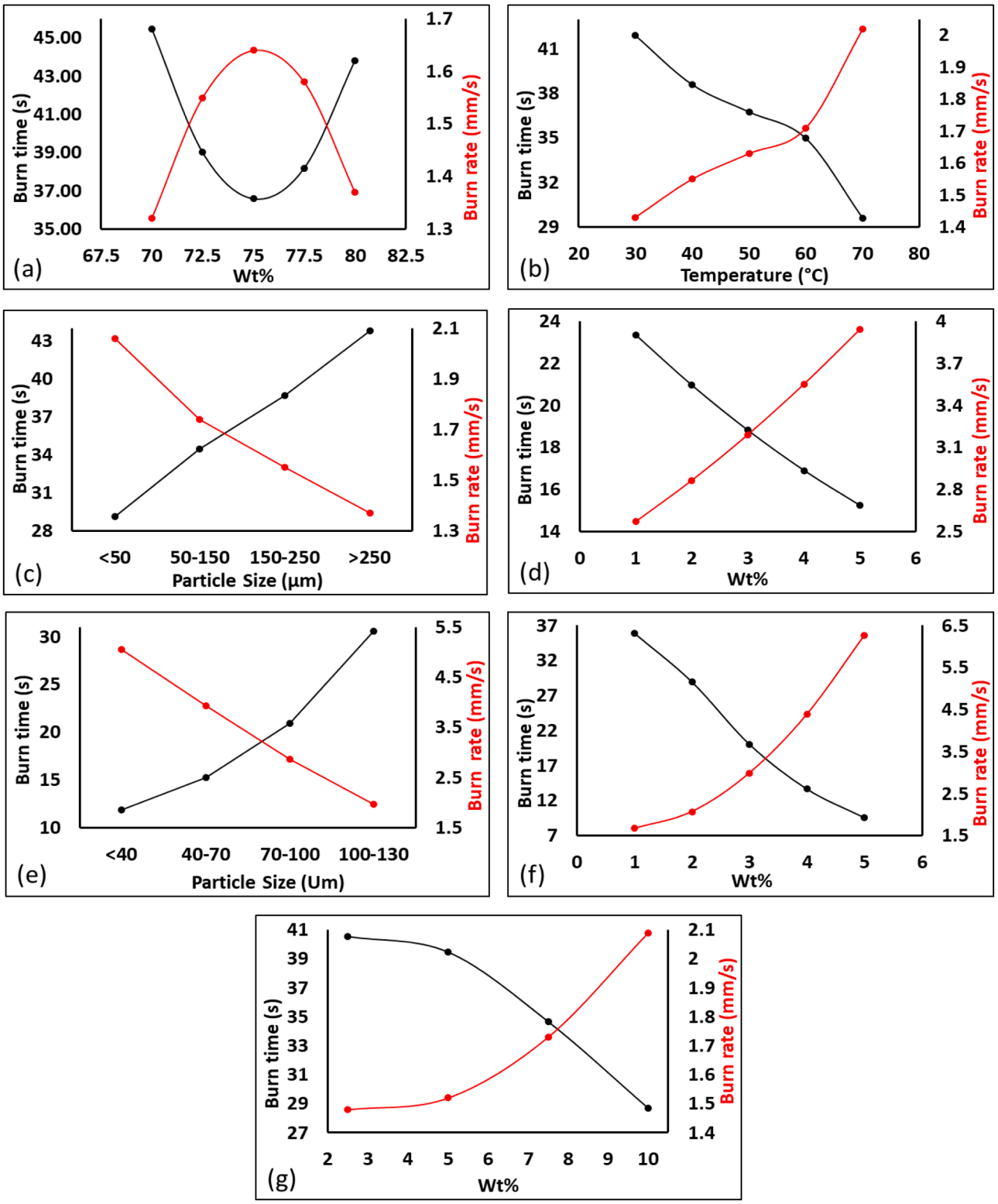

Fig. 3. Burn rate and Burn time for (a) Different weight percent of oxidizer, (b) Various ambient temperatures, (c) Effects of oxidizer's particle size, (d) Different weight percent of $CuCr_2O_4$, (e) Various particle sizes for $CuCr_2O_4$, (f) Different weight percent of Fe_2O_3, (g) Different weight percent of Aluminum.

hot, dense molten metal enhances both conductive and radiative heat transfer, further promoting rapid flame spread [36]. When the formulation included excess Fe_2O_3 ($\Phi = 0.59$), the burn rate increased further to 2.78 mm/s, representing a 110.61 % enhancement over the baseline composition. This enhancement results from the combined catalytic effects of iron oxide and the heat transfer benefits of the thermite reaction products. These thermodynamic and kinetic interactions align well with the experimentally observed performance gains in thermite-containing formulations.

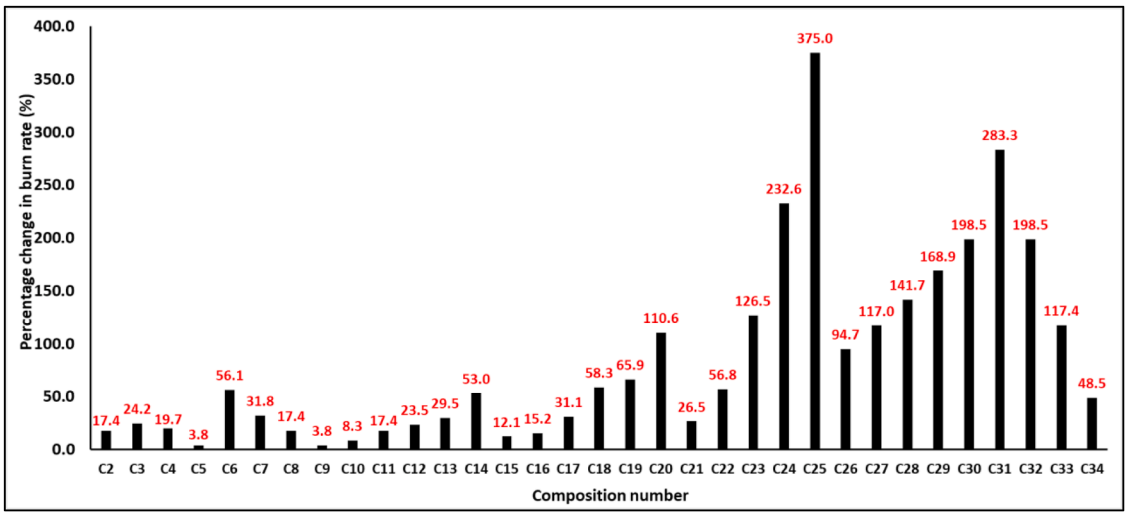

Fig. 4. Percentage change in the burn rate for all the compositions (rounded off to one decimal point for ease of plotting).

3.2. Density and mass flow

The density of solid propellant plays a crucial role in the thrust (F) production, as thrust is a function of the mass flow rate ($\dot{m}$) and the exhaust velocity (V_e). The mass flow rate of the high-pressure combustion gases is directly proportional to burn rate (BR), propellant density (ρ_p) and the burning surface area (A_b). These relationships are presented in the Eq. (3), (4), (5) below [1].

$$\dot{m} = \rho_p * BR * A_b \tag{3}$$

$$F = V_e * \dot{m} \tag{4}$$

$$F = V_e * \rho_p * BR * A_b \tag{5}$$

A higher propellant density enables a greater mass of fuel to be packed into a given space which allow more mass to be burned per unit volume, thereby increasing the mass flow rate, and ultimately enhancing thrust. This not only allows for more compact and powerful rocket or missile designs, but also improves the burn time, leading to a higher impulse per unit volume and greater energy output. Consequently, optimizing density is essential for efficient propulsion system performance, especially in dimensionally restricted applications [37].

Theoretical calculations were done to obtain the density of all the compositions having various additives with different loadings to systematically study the effect on the density of AP-PVC-based solid propellant strands. Table 7 represents the density values for enhanced composition with additives, and Fig. 5 presents the percentage change in the density of different compositions due to different wt. % of various additives studied in this work. The maximum density changes of 11.59 % were observed for composition 20, which had Al and Fe_2O_3. The density went from 1.785 g/cm^3 to 2.78 g/cm^3, demonstrating the synergistic effect of dual additives. A clear trend was observed with the variation in oxidizer-to-fuel ratio, where increasing the oxidizer content from 70 % to 80 % in composition 1 to composition 5, leading to a steady increase in density from 1.785 g/cm^3 to 1.840 g/cm^3. This indicates the role of higher oxidizer loading in densifying the propellant matrix, with an increase of 3.08 % in the density. The addition of Al in compositions 15 to 18 showed a linear increase in density, rising from 1.82 % to 7.28 % as the Al content increased from 2.5 % to 10 %. Further, the compositions with only Fe_2O_3, i.e., compositions 21 to 25, revealed a gradual density increase from 0.73 % to 3.64 % as wt. % of Fe_2O_3 in the composition increased from 1 % to 5 %. Similarly, $CuCr_2O_4$ addition in Compositions 26–30 resulted in significant density enhancements from 1.51 % to 7.56 %.

Table 7
Density and the mass flow rate for the compositions of interest.

Composition ID	Density (g/cm^3)	Burning surface area (m^2)	Mass flow rate (kg/s)
C 1	*1.78*		*0.008482*
C 2	1.79		0.010037
C 3	1.81		0.010701
C 4	1.83		0.010388
C 5	1.84		0.009075
C 15	1.82		0.009684
C 16	1.85		0.010123
C 17	1.88		0.011724
C 18	1.92		0.014408
C 19	1.80		0.014175
C 20	1.81	*0.0036*	0.018124
C 21	1.82		0.010966
C 22	1.84		0.013689
C 23	1.85		0.019913
C 24	1.93		0.030451
C 25	1.99		0.044959
C 26	1.81		0.016765
C 27	1.84		0.018934
C 28	1.87		0.021429
C 29	1.89		0.024193
C 30	1.92		0.027233

These results indicate that incorporating metal-based additives significantly improves propellant strand density, with dual-metal systems (Al + Fe_2O_3) being particularly effective. The lowest change in density was seen when the oxidizer loading was changed, though not significant, but there was an increase. Enhanced density is likely due to improved packing efficiency and interfacial bonding between additives and binder matrix, contributing to better structural integrity, uniform burning, and improved energetic performance. The mass flow rate for the compositions was calculated using the density and burn rate data and is tabulated Table 7.

The burning area of the propellant strand was 0.0036 m^2, which was used to calculate the mass flow rate. The calculated mass flow rate results, shown in Table 7, reveal strong correlations with both burn rate and density. As expected from Eq. (3), compositions with higher densities and faster burn rates exhibited significantly higher mass flow rates. For example, composition C25, which had the highest burn rate (6.27 mm/s) and density (1.99 g/cm3), also recorded the highest mass flow rate of 0.04496 kg/s. In contrast, the base composition C1 had a much lower mass flow rate of 0.00848 kg/s. This trend underscores the importance of simultaneously optimizing burn rate and density when

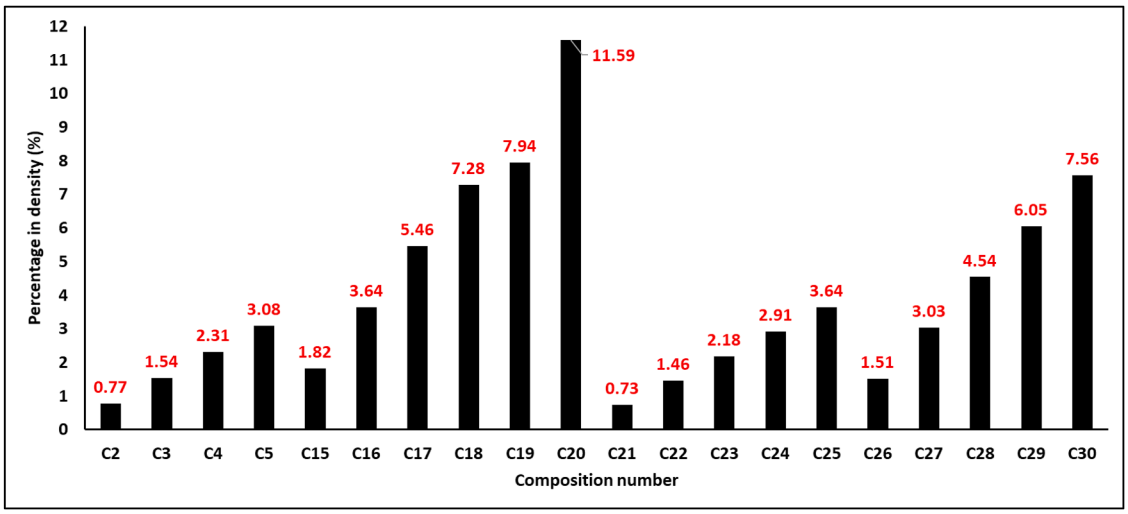

Fig. 5. Percentage change in density for all the compositions.

designing high-thrust propellant formulations. Additives like Fe_2O_3 and $CuCr_2O_4$, when used in appropriate weight percentages and particle sizes, not only enhance reaction kinetics but also contribute significantly to the overall propellant mass flow, thereby improving thrust potential.

3.3. Adiabatic flame temperature

The Adiabatic Flame Temperature for the compositions of interest was simulated and calculated using the CEARUN program that works on the equilibrium and thermodynamic calculations done by NASA CEA (Chemical Equilibrium with Applications). It is a widely used computational tool that models the chemical equilibrium of combustion reactions by taking the user's inputs, like ambient pressure and temperature, and the reactants along with their ratios in the composition. For each propellant composition, the oxidizer-to-fuel ratio and composition-specific details were entered into the NASA CEA software. The chemical equilibrium composition of a mixture of product gases at the input temperature and pressure was computed, and the corresponding temperature under adiabatic conditions was obtained. The Adiabatic Flame Temperature values for the different compositions, thus calculated, are presented in Table 6. The temperatures range from 1810 K for the composition with 1 % of Fe_2O_3 to 3139 K for the composition with 10 % of aluminum in the formulation. Fig. 6 illustrates the graphical representation of AFT to analyze the trends. The variation in the AFT of the tested compositions reflects the alteration in the combustion efficiencies and energy outputs due to the addition of different kinds of additives and their loading in the compositions [38].

The base composition exhibited an AFT of 2652.31 K. As the oxidizer-to-fuel ratio was varied, the AFT increased, peaking at 2704.37 K for composition 3, having 75 % oxidizer loading. When the oxidizer content was further increased to 80 %, the AFT dropped to 2670.55 K. This can be inferred to the fact the extra oxidizer started absorbing more heat for its own decomposition but didn't significantly contribute to the combustion process. Also, increasing the oxidizer meant reduction in PVC content of the composition, which further reduced the fuel available for combustion. A similar trend of increasing till a point and then decreasing can be seen for both the burn rate as well as AFT of the compositions 1 to 5. The effect of ambient temperature variations on AFT, though, was minor (AFT difference ranging between 2.5 and 3) but followed a specific pattern. A gradual increase from 2653.25 K for composition 10, which was at 30 °C, to 2663.97 K for composition 14 at 70 °C was observed. This indicates a minor thermal enhancement with

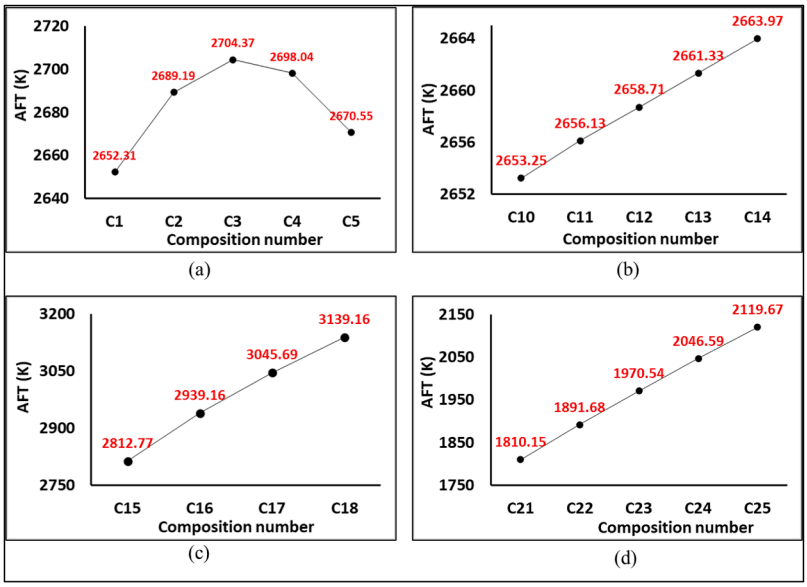

Fig. 6. Adiabatic flame temperature calculated using NASA CEA (a) wt. % of oxidizer (b) Ambient temperature (c) wt. % of Al (d) wt. % of Fe_2O_3.

rising environmental temperature [39]. Ambient temperature does not affect the AFT significantly, but it does accelerate the combustion phenomenon as discussed previously.

Compositions 15 to 18 had been enhanced with aluminum as additives. These showed a consistent rise in AFT with increasing aluminum wt. %, culminating in a maximum AFT of 3139.16 K for composition 18 that had 10 % of Al powder. This trend is attributed to the high energy density of aluminum that enables it to produce high thermal output [40]. Interestingly, adding two different combinations of aluminum and iron oxide in compositions 19 and 20 led to significantly lower AFTs compared to the counterpart compositions with only aluminum. Composition 20, which had 10 % Al and 2 % Fe_2O_3, exhibited an AFT of 2063.14 K. This drop is possibly due to the catalytic effect of Fe_2O_3 on the decomposition of ammonium perchlorate (AP), which accelerates the combustion of PVC using the available oxygen, thereby leaving insufficient oxygen for the complete combustion of aluminum. Since PVC burns at relatively low temperatures compared to the activation energy required for aluminum, aluminum may remain unreacted or only partially oxidized [11,31] . The hot gaseous products from PVC combustion (primarily CO_2, CO, and H_2O) can react with and oxidize aluminum. Condensed phase alumina (Al_2O_3) is produced as the result of this reaction, which acts as a heat sink absorbing a significant amount of heat and ultimately lowering the adiabatic flame temperature (AFT) [41]. Compositions 21 to 25, with increasing Fe_2O_3 content alone, followed an ascending trend in AFT values, rising from 1810.15 K to 2119.67 K. Compared to the base composition, the adiabatic flame temperature (AFT) is significantly lower. This reduction is primarily due to the heat-absorbing nature of ceramic oxides. While these additives enhance the reaction kinetics by acting as catalysts, they simultaneously reduce the thermodynamic output. In particular, the redox cycling of iron oxide serves as a heat sink mechanism, absorbing thermal energy during its reduction and oxidation transitions. Thereby, it lowers the overall flame temperature and, in some cases, partially quenches the flame [42]. The increase in the AFT with increasing wt. % of Fe_2O_3 can be attributed to the mechanism of enhanced decomposition of the oxidizer, leading to an accelerated combustion reaction with PVC as already discussed in the previous sections.

To further interpret the AFT trends and support the above claims, the oxygen balance (OB %) of selected formulations was estimated. As shown in Fig. 7, compositions with more negative OB % (fuel-rich, such as C18 with 10 % Al) exhibited significantly higher flame temperatures, peaking at over 3100 K. This is attributed to the high enthalpy of aluminum combustion and limited dilution by oxidizer by-products. In contrast, oxidizer-rich or balanced systems like C3 and C25 yielded moderate AFTs, while thermite-based compositions (e.g., C20) showed slightly reduced flame temperatures despite their exothermic nature. This reduction can be attributed to heat sink effects from refractory residues such as Fe and Al_2O_3, which do not fully contribute to gas-phase combustion temperature. These findings highlight that OB %, in conjunction with additive phase behavior, significantly influences thermal characteristics.

3.4. Summary for optimal formulations

To guide future formulation strategies, a summary of the most effective additive loadings based on burn rate, adiabatic flame temperature, density, and calculated mass flow rate is provided in Table 8. These optimal values were identified from the broad range of tested compositions in this study.

To visually assess performance trade-offs, a comparative radar chart was constructed using normalized values of burn rate, density, AFT, and mass flow rate for key compositions (Fig. 8). This representation illustrates how compositions with high thermal output (e.g., C18 with 10 % Al) differ from those optimized for burn rate or flow rate (e.g., C25 with 5 % Fe_2O_3). Such visualization can aid in selecting formulations tailored to specific propulsion requirements.

To assess the practical propulsion potential of selected propellant

Table 8
Summary of optimal formulations derived from experimental results.

Additive System	Optimum Loading (wt. %)	Max Burn Rate (mm/s)	Max AFT (K)	Max Density (g/cm3)	Max Mass Flow Rate (kg/s)
Fe_2O_3 only	5	6.27	2119.67	1.99	0.04496
Al only	10	2.08	3139.16	1.92	0.01441
$CuCr_2O_4$ only	5	3.94	N/A	1.92	0.02723
Thermite (Al + Fe_2O_3)	10 + 2	2.78	2063.14	1.81	0.01812

Note: *AFT values for* $CuCr_2O_4$ *compositions are not reported due to the lack of thermochemical data in the NASA CEA database. However, significant burn rate and density improvements validate its effectiveness.*

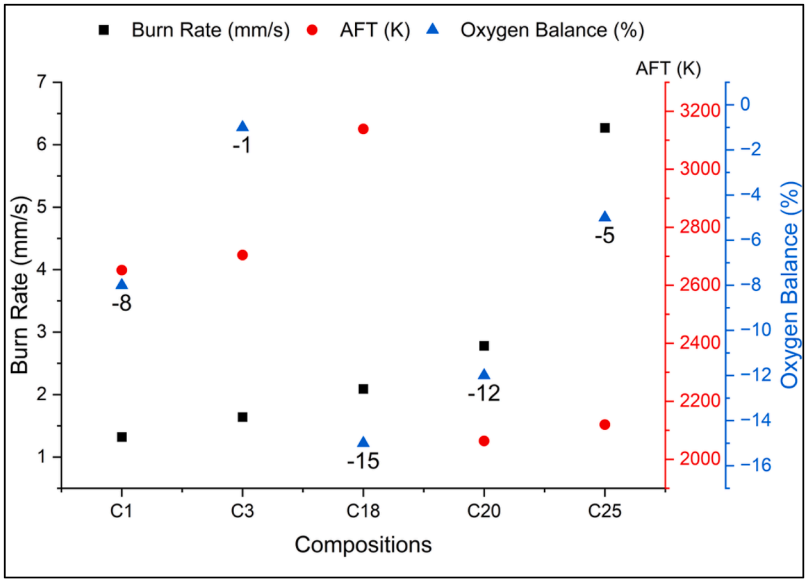

Fig. 7. Correlation of AFT, burn rate with oxygen balance (OB %).

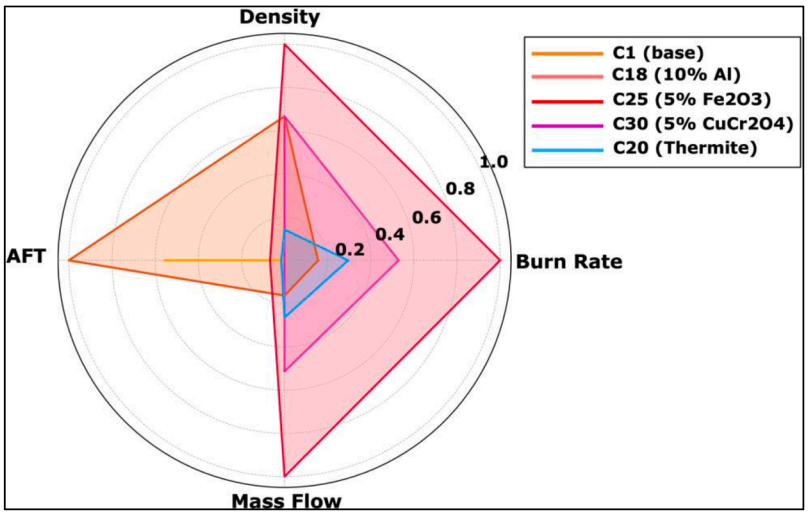

Fig. 8. Normalized performance comparison of selected compositions.

compositions, an ideal thrust estimation was performed using calculated mass flow rates and adiabatic flame temperatures. Assuming a chamber pressure of 20 bar, an exit pressure of 1 atm, and an average molar mass of 30 kg/kmol, the theoretical exhaust velocities and thrust were estimated using isentropic nozzle flow Eqs. (6) and (7).

$$F = \dot{m} \cdot V_e \tag{6}$$

$$V_e = \sqrt{\frac{2\gamma RT}{\gamma - 1}\left[1 - \left(\frac{P_e}{P_c}\right)^{\frac{\gamma-1}{\gamma}}\right]} \tag{7}$$

where, γ is the specific heat ratio, R is the universal gas constant, T is the AFT, P_e and P_c are the exit and chamber pressures respectively, V_e is the exit velocity, F is the thrust, $\dot{m}$ is the mass flow rate. Results in Table 9 show that C25 (5 % Fe_2O_3) produced the highest thrust at 73.04 N, largely due to its exceptional burn rate and high mass flow. Despite a lower AFT, the composition benefits from efficient redox balance and favorable density. In contrast, C18 (10 % Al) demonstrated a higher thermal output but lower mass flow, yielding only moderate thrust. These results underscore the need to optimize both energetic content and combustion dynamics for practical propulsion use.

Table 9
Thrust Estimation for four compositions using ideal rocket theory.

Composition	AFT (K)	Mass Flow (kg/s)	Exit Velocity (m/s)	Estimated Thrust (N)
C1	2652.31	0.00848	1817.24	15.41
C18	3139.16	0.01441	1977.00	28.49
C20	2063.14	0.01812	1602.74	29.04
C25	2119.67	0.04496	1624.55	**73.04**

4. Conclusion

This study provides a comprehensive experimental analysis of how additive loading levels, particle sizes, and redox combinations affect the performance of PVC/AP-based composite propellants. Rather than proposing new additive chemistries, the novelty lies in the systematic coverage of a wide range of additive types, namely Al, Fe_2O_3, $CuCr_2O_4$, and thermite systems, and their influence on burn rate, density, AFT, and mass flow rate. The study bridges a critical gap in the literature by going beyond single-point testing and offering a comparative dataset across more than 30 compositions. The major outcomes from this research are listed below:

1. Finer additive particles and higher loading levels consistently led to faster burn rates and higher mass flow, reflecting the catalytic enhancement from increased surface area and reactive mass.
2. Radar charts visualize all key metrics together for each formulation, highlighting trade-offs. For example, compositions with the highest burn rates also tended to have higher densities, illustrating a trade-off between combustion speed and propellant mass.
3. The calculated enthalpy of the Al+Fe_2O_3 thermite reaction (–851.5 kJ/mol) confirms a strong exothermic energy release. This large energy boost explains the higher flame temperatures and burn rates observed in thermite-containing propellants, confirming enhanced combustion.
4. Calculated oxidizer-balance percentages explain variations in AFT and burn rate. Formulations near stoichiometric OB exhibited higher adiabatic flame temperatures and faster burn rates, showing an optimal fuel–oxidizer ratio, whereas off-balance mixtures performed less efficiently.
5. Theoretical thrust calculations showed the highest thrust (~73 N) for the Fe_2O_3-rich "C25" formulation. This matches expectations that Fe_2O_3 additives yield the greatest propulsion performance, validating the enhanced thrust of that formulation.

Future work could incorporate advanced thermal analysis (DSC/TGA) and performance simulations, such as nozzle modeling, to complement and extend the findings. The dataset also holds potential for application in machine learning-based optimization tools.

CRediT authorship contribution statement

Lakshay Bansal: Formal analysis, Investigation, Software, Validation, Visualization, Writing – original draft. **Prakhar Jindal:** Conceptualization, Data curation, Formal analysis, Methodology, Project administration, Resources, Supervision, Visualization, Writing – review & editing.

Declaration of competing interest

The authors declare that they have no known competing financial interests or personal relationships that could have appeared to influence the work reported in this paper.

Data availability

Data will be made available on request.

References

[1] G.P. Sutton, O. Biblarz, Rocket Propulsion Elements, 8th ed., John Wiley & Sons, 2010.

[2] R. Nagappa, M.R. Kurup, A.E. Muthunayagam, ISRO's solid rocket motors, Acta Astronaut. 19 (8) (Aug. 1989) 681–697, https://doi.org/10.1016/0094-5765(89)90136-7.

[3] I.N. Yaacob, et al., A review on viscoelastic behaviour of plasticizers in ap/al/htpb based composite solid propellant, Mater. Today Proc. (2023), https://doi.org/10.1016/j.matpr.2023.01.176.

[4] S. Whalen, E. Sellards, B. Gobin, G. Young, Exploring the influence of additives on the ignition, combustion and quenching of electrically controlled solid propellants, Propell. Explos. Pyrotech. 49 (6) (Jun. 2024), https://doi.org/10.1002/prep.202300299.

[5] M.Z. Azizi, et al., Heat of combustion and thermal decomposition of ammonium perchlorate/sorbitol solid propellant with metal additives, J. Adv. Res. Exp. Fluid Mech. Heat Transf. 18 (1) (Jan. 2025) 94–105, https://doi.org/10.37934/arefmht.18.1.94105.

[6] L. Bansal, P. Jindal, V.Kumar Rathi, A critical review of limitations and challenges in advancement of HNF as a green oxidizer for composite solid propellant formulations, Propell. Explos. Pyrotech. (May 2025), https://doi.org/10.1002/prep.12072.

[7] P. Kumar, An overview on properties, thermal decomposition, and combustion behavior of ADN and ADN based solid propellants, Def. Technol. 14 (6) (2018) 661–673, https://doi.org/10.1016/j.dt.2018.03.009.

[8] V.P. Sinditskii, V.Y. Egorshev, M.V. Berezin, Study on combustion of new energetic nitramines, in: Int. Annu. Conf. ICT 32nd, 2001, pp. 59/1–59/13.

[9] V.P. Sinditskii, V.Y. Egorshev, A.I. Levshenkov, V.V. Serushkin, Ammonium nitrate: combustion mechanism and the role of additives, Propell. Explos. Pyrotech. 30 (4) (2005) 269–280, https://doi.org/10.1002/prep.200500017.

[10] Y. Wang, X. Song, F. Li, Thermal behavior and decomposition mechanism of ammonium perchlorate and ammonium nitrate in the presence of nanometer triaminoguanidine nitrate, ACS Omega 4 (1) (2019) 214–225, https://doi.org/10.1021/acsomega.8b02515.

[11] A. Manash, P. Kumar, Comparison of burn rate and thermal decomposition of AP as oxidizer and PVC and HTPB as fuel binder based composite solid propellants, Chin. Ord. Soc. (2019), https://doi.org/10.1016/j.dt.2018.08.010.

[12] P. Jain, V.K. Rathi, S. Biswas, Study of aging characteristics for metalized HTPB based composite solid propellants stored in ambient conditions, Def. Sci. J. 74 (5) (Aug. 2024) 615–626, https://doi.org/10.14429/dsj.74.19786.

[13] M. Abbas, R. Kumar, S. Biswas, Effect on the performance of a hybrid rocket using AP in the PVC and HTPB-based hybrid fuel, FirePhysChem (Aug. 2024), https://doi.org/10.1016/j.fpc.2024.08.004.

[14] D. Ka, et al., Mechanical and combustion properties of fluoroalkylsilane surface-functionalized boron/HTPB composite, Combust. Flame 268 (Oct. 2024), https://doi.org/10.1016/j.combustflame.2024.113621.

[15] W.Q. Pang, R.A. Yetter, L.T. DeLuca, V. Zarko, A. Gany, and X.H. Zhang, "Boron-based composite energetic materials (B-CEMs): preparation, combustion and applications," Nov. 01, 2022, Elsevier Ltd. doi: 10.1016/j.pecs.2022.101038.

[16] A. Manash, P. Kumar, Comparison of burn rate and thermal decomposition of AP as oxidizer and PVC and HTPB as fuel binder based composite solid propellants, Chin. Ord. Soc. (2019), https://doi.org/10.1016/j.dt.2018.08.010.

[17] H. Tian, Z. Wang, Z. Guo, R. Yu, G. Cai, Y. Zhang, Effect of metal and metalloid solid-fuel additives on performance and nozzle ablation in a hydroxy-terminated polybutadiene based hybrid rocket motor, Aerosp. Sci. Technol. 123 (Apr. 2022), https://doi.org/10.1016/j.ast.2022.107493.

[18] P.N. Dave, R. Sirach, An efficient nanocatalyst cobalt copper zinc ferrite for the thermolysis of ammonium nitrate, ACS Omega 7 (48) (Dec. 2022) 43784–43792, https://doi.org/10.1021/acsomega.2c04796.

[19] T. Mitani, M. Izumikawa, Combustion efficiencies of aluminum and boron in solid propellants, J. Spacecr. Rockets 28 (1) (1991) 79–84, https://doi.org/10.2514/3.26212.

[20] B. Gou, et al., Effect of nano-copper chromite on the thermal decomposition and combustion of AP-based solid propellants, Propell. Explos. Pyrotech. 47 (10) (Oct. 2022), https://doi.org/10.1002/prep.202200087.

[21] M. Li, Z. Han, L. Jiang, G. Xu, Study on combustion characteristics and pyrotechnic cutting effects of bimetal thermite Ni/Al/Fe2O3 system, Propell. Explos. Pyrotech. 49 (5) (May 2024), https://doi.org/10.1002/prep.202300285.

[22] D.A. Reese, D.M. Wright, S.F. Son, CuO/Al thermites for solid rocket motor ignition, J. Propuls. Power 29 (5) (2013) 1194–1199, https://doi.org/10.2514/1.B34771.

[23] H. Shekhar, Effect of temperature on mechanical properties of solid rocket propellants, Def. Sci. J. 61 (6) (2011) 529–533, https://doi.org/10.14429/dsj.61.774.

[24] N.S. Cohen, D.A. Flanigan, Mechanisms and models of solid-propellant burn rate temperature sensitivity - a review, AIAA J. 23 (10) (Oct. 1985) 1538–1547, https://doi.org/10.2514/3.9121.

[25] M.K. Bharti, L. Bansal, S. Chalia, Catalytic potential of microsized additives in enhancing the linear burn rate of potassium nitrate-sucrose based composite solid propellant strands, Int. J. Energ. Mater. Chem. Propuls. 20 (4) (2021) 61–77, https://doi.org/10.1615/IntJEnergeticMaterialsChemProp.2021038209.

[26] S. Isert, T.D. Hedman, R.P. Lucht, S.F. Son, Oxidizer coarse-to-fine ratio effect on microscale flame structure in a bimodal composite propellant, Combust. Flame 163 (Jan. 2016) 406–413, https://doi.org/10.1016/j.combustflame.2015.10.015.

[27] J.C. Oxley, J.L. Smith, M. Donnelly, M. Porter, Fuel-oxidizer mixtures: their stabilities and burn characteristics, J. Therm. Anal. Calorim. 121 (2) (Aug. 2015) 743–763, https://doi.org/10.1007/s10973-015-4589-x.

[28] N.N. Bakhman, Dependence of burning rate on oxidizer particle size, Combust. Flame 17 (3) (Dec. 1971) 383–389, https://doi.org/10.1016/S0010-2180(71)80061-5.

[29] A.P. Sanoop, R. Rajeev, B.K. George, Synthesis and characterization of a novel copper chromite catalyst for the thermal decomposition of ammonium perchlorate, Thermochim. Acta 606 (Apr. 2015) 34–40, https://doi.org/10.1016/j.tca.2015.03.006.

[30] P.R. Patil, V.N. Krishnamurthy, S.S. Joshi, Effect of nano-copper oxide and copper chromite on the thermal decomposition of ammonium perchlorate, Propell. Explos. Pyrotech. 33 (4) (Aug. 2008) 266–270, https://doi.org/10.1002/prep.200700242.

[31] F. Maggi, et al., Iron oxide as solid propellant catalyst: a detailed characterization, Acta Astronaut. 158 (May 2019) 416–424, https://doi.org/10.1016/j.actaastro.2018.07.037.

[32] T. Mattisson, A. Lyngfelt, P. Cho, The use of iron oxide as an oxygen carrier in chemical-looping combustion of methane with inherent separation of CO2, Fuel 80 (13) (Oct. 2001) 1953–1962, https://doi.org/10.1016/S0016-2361(01)00051-5.

[33] A.G. Korotkikh, D.V. Teplov, I.V. Sorokin, Combustion features of dispersed aluminum and boron in high-energy composition, FirePhysChem 4 (4) (Dec. 2024) 277–282, https://doi.org/10.1016/j.fpc.2024.03.002.

[34] R.A. Yetter, G.A. Risha, S.F. Son, Metal particle combustion and nanotechnology, in: Proceedings of the Combustion Institute 32 II, 2009, pp. 1819–1838, https://doi.org/10.1016/j.proci.2008.08.013.

[35] J. Glorian, S. Gallier, L. Catoire, On the role of heterogeneous reactions in aluminum combustion, Combust. Flame 168 (Jun. 2016) 378–392, https://doi.org/10.1016/j.combustflame.2016.01.022.

[36] Z. Hu, W. Ding, J. Chen, T. Guo, D. Zhang, L. Xie, Preparation and characterization of modified Al/Fe2O3 nano-thermite composite system, J. Therm. Anal. Calorim (2024), https://doi.org/10.1007/s10973-024-13695-3.

[37] S. Verma, P.A. Ramakrishna, Dependence of density and burning rate of composite solid propellant on mixer size, Acta Astronaut. 93 (2014) 130–137, https://doi.org/10.1016/j.actaastro.2013.07.016.

[38] C.Y. Cao, D. Zhang, C.C. Liu, S. Lu, H.P. Zhang, Experimental investigation on combustion behaviors and reaction mechanisms for 5-aminotetrazole solid propellant with nanosized metal oxide additives under elevated pressure conditions, Appl. Therm. Eng. 162 (Nov. 2019), https://doi.org/10.1016/j.applthermaleng.2019.114207.

[39] A.I. Atwood, et al., Burning rate of solid propellant ingredients, part 1: pressure and initial temperature effects, J. Propuls. Power 15 (6) (1999) 740–747, https://doi.org/10.2514/2.5522.

[40] R.A. Yetter, G.A. Risha, S.F. Son, Metal particle combustion and nanotechnology, in: Proceedings of the Combustion Institute 32 II, 2009, pp. 1819–1838, https://doi.org/10.1016/j.proci.2008.08.013.

[41] A. Sözen, E. Özbaş, T. Menlik, M.T. Çakir, M. Gürü, K. Boran, Improving the thermal performance of diffusion absorption refrigeration system with alumina nanofluids: an experimental study, Int. J. Refrig. 44 (2014) 73–80, https://doi.org/10.1016/j.ijrefrig.2014.04.018.

[42] H.I. Joo, K. Duncan, G. Ciccarelli, Flame-quenching performance of ceramic foam. Combustion Science and Technology, Dec. 2006, pp. 1755–1769, https://doi.org/10.1080/00102200600788692.